Processing and Application of Ceramics 8 [4] (2014) 211–218
DOI: 10.2298/PAC1404211O

Synthesis, structure and magnetic properties of $Y_3Fe_{5-x}Al_xO_{12}$ garnets prepared by the soft chemical method

Pedro Paulo Silva Ortega[1], Miguel Angel Ramirez[1], César Renato Foschini[2], Filiberto González Garcia[3], Mario Cilense[4], Alexandre Zirpoli Simões[1,*]

[1]*Universidade Estadual Paulista - UNESP, Faculdade de Engenharia de Guaratinguetá, Av. Dr. Ariberto Pereira da Cunha, 333, Bairro Portal das Colinas, CEP 12516-410, Guaratinguetá, SP, Brazil*
[2]*Universidade Estadual Paulista - UNESP, Faculdade de Engenharia de Bauru, Dept. de Eng. Mecânica, Av. Eng. Luiz Edmundo C. Coube 14-01, Zip-Code: 17033-360, Bauru, SP, Brazil*
[3]*Universidade Federal de Itajubá, Instituto de Física e Química, Ave. BPS 1303, Itajubá, 37500-903, Minas Gerais, MG, Brazil*
[4]*Universidade Estadual Paulista - UNESP- Instituto de Química – Laboratório Interdisciplinar em Cerâmica (LIEC), Rua Professor Francisco Degni s/n, Zip-Code: 14800-90-, Araraquara, SP, Brazil*

Received 13 October 2014; Received in revised form 19 December 2014; Accepted 22 December 2014

Abstract

A study was undertaken about the structural, morphological and magnetic properties at room temperature of crystalline aluminium substituted yttrium iron garnet, YIG ($Y_3Fe_{5-x}Al_xO_{12}$ with $1.5 < x < 1.7$) nanoparticles prepared by polymeric precursor method at the temperature of 700 °C for 2 hours. The single-phase character and the well-defined structure of YIG nanoparticles were confirmed by X-ray diffraction, excluding the presence of any other phases. The Raman spectra showed that the changes of lattice vibration would influence interaction between the Fe ion and the host. Mean crystallite size of the single-phase powder was about 46–65 nm. Particles' morphology was investigated by high-resolution transmission electron microscopy, which shows that the particles were agglomerated. From hysteresis loops, particles' efficiency range from 91.4% to 95.9% as Fe/Al ratio decreases. Saturation magnetization was affected by the particle size and Fe/Al stoichiometric ratio. We observe that the saturation magnetization increases as the Fe/Al ratio is raised due to enhancement of the surface spin effects.

Keywords: *yttrium iron garnet, powder, chemical synthesis, characterization, magnetic properties*

I. Introduction

In recent years, hyperthermia a therapeutic procedure used in cancer treatment has been the subject of extensively studies. It is based in the principle that temperatures around 42 °C destroy cancerous cells preserving the surrounding healthy tissues, once the malignant cells are less resistant to this increase in temperature [1]. Hyperthermia has a notable lack of side effects, which makes it an attractive substitute or combined treatment for chemotherapy and radiotherapy. Though many distinct modes of hyperthermia are available, such as electromagnetic radiation, lasers, microwaves and radiofrequency, they have serious limitations in tumor targeting and precise localization of the thermal energy [2,3]. Therefore, the ideal mechanism for a proper use in hyperthermia must be capable of heating the cancer site affecting the less possible the surrounding healthy tissues. Gilchrist *et al.* [4] suggested that the selectivity required can be achieved through a powdered magnetic material with controlled particle size which must be one micron or less in diameter. Hence, the magnetic particles can be guided or localized in a specific target through an external magnetic field [1]. Kumar's recent review [5] pointed out many types of magnetic materials that have been studied for their hyperthermia potential, most of them iron oxide-based materials. As it is known, the iron-containing oxide phases

* Corresponding author: tel: +55 12 3123 2228
e-mail: *alezipo@yahoo.com*

with $A_3B_5O_{12}$ cubic garnet structure possess unique magnetic, magneto-optical, thermal, electrical and mechanical properties, such as ferrimagnetism, excellent creep, high thermal conductivity, high electrical resistivity, moderate thermal expansion coefficients, radiation damage resistance, energy-transfer efficiency and controllable magnetization saturation. [6] Yttrium iron garnets (YIG), $Y_3Fe_5O_{12}$, belong to this class of materials. Since their discovery in 1956 by Bertaut and Forrat [7], YIG have attracted attention due to their interesting properties, as low dielectric loss, narrow resonance linewidth in microwave region and good saturated magnetization value [8], and as an important material in optical communication and magneto-optical devices [6–10]. YIG crystallizes in cubic structure, space group *Ia3d*, with eight molecules in a unit cell of lattice constant $a = 12.376 \pm 0.004$ Å [10]. There are three sublattices: tetrahedral (*d*), octahedral (*a*) and dodecahedral (*c*). They are surrounded by four, six and eight oxygen ions, respectively. The formula unit can be written as $Y_3Fe_2(FeO_4)_3$ and yttrium ions occupy 24*c* (dodecahedral) sites, two iron ions occupy 16*a* (octahedral) sites and the other three iron ions occupy 24*d* (tetrahedral) sites. The only magnetic ion in YIG is Fe^{3+}. A magnetic moment of 5 μB per formula unit results from antiferromagnetic superexchange interaction between these Fe^{3+} ions in octahedral and tetrahedral sites through the intervening O^{2-} ions [6,10,11]. Akhtar *et al.* [12] showed that magnetic properties (such as remanence and saturation) depend on particle size, magnetic dilution and superexchange interaction of the YIG ferrites. Although YIG high saturated magnetization value is significant for hyperthermia, its controllable Curie temperature, T_c (or Curie point) is an equally important property. Above Curie temperature ferromagnetic material becomes paramagnetic. When exposed to an external magnetic field, YIG generates heat due to both Neel and Brown relaxation [13]. Once these particles reach Curie temperature they no longer generate heat. This phenomenon prevents the particles from overheating and damaging human tissues. The substitution of metal ions in the ferrite structure can affect the magnetic, electrical and dielectric properties of ferrites [14]. As Grasset *et al.* demonstrated [15], aluminium substituted YIG ($Y_3Fe_{5-x}Al_xO_{12}$, $0 \leq x \leq 2$) decreases Curie point near body temperature by adjusting Fe/Al ratio, making these particles self-regulated and safe-guarded for hyperthermia applications. A variety of synthesis methods for obtaining YIG has been described in literature, such as the mechanochemical method [11], solid state reaction [16], citrate sol-gel [17], microwave-induced combustion [18], hydroxide coprecipitation [19], coprecipitation in microemulsion [20], metal alkoxides hydrolysis [21], glycothermal synthesis [22] and glass-crystallization [23]. Although, in literature was found that only the hydroxide coprecipitation method perform aluminium substituted YIG. In this paper, polymeric precursor method, or Pechini method, was used to synthesize aluminium substituted YIG, $Y_3Fe_{5-x}Al_xO_{12}$ ($1.5 < x < 1.7$), which has not yet been reported in literature. This technique was originally developed by Maggio Pechini in 1967 [24]. It is based on the chelation of a metallic cation by a carboxylic acid, such as citric acid, and further polymerization promoted by the addition of ethylene glycol and consequent polyesterification [25]. This method possesses important advantages: possibility of working with aqueous solutions, synthesis at low temperatures free of contamination, low cost, no necessity of high atmosphere control, good stoichiometric control at a molecular level and produces powders in a nanometric scale [26–28].

II. Experimental procedure

The reactants used were all reagent grade: $Y(NO_3)_3{\times}6\,H_2O$ (99.9%) and $AlC_5H_5O_7$ (99.9%) were provided by Aldrich, $FeC_6H_5O_7{\times}NH_4OH$ (99.5%) by Merck, and $C_6H_8O_7$ (99.5%) and $C_2H_6O_2$ (99.5%) by Synth. The polycrystalline nanoparticles of the composition $Y_3Fe_{5-x}Al_xO_{12}$ with $1.5 < x < 1.7$ were prepared by the polymeric precursor method. All reagents were weighed according to the previous defined stoichiometries. The resins were obtained dissolving ammonium iron (III) citrate, yttrium nitrate hexahydrate and aluminium citrate in water by constant mixing at 80 °C. Afterwards, citric acid and ethylene glycol were added to the solution. Citric acid complex the metal ions and ethylene glycol promotes the polymerization. The result is a yellow coloured, clear, homogeneous polyester resin. Alumina crucibles were used for calcination of each resin. The first part consisted of preparing a metal-citrate complex for three different stoichiometries, with *x* values equal to 1.5, 1.6 and 1.7. The second part was to decompose the organic material at 700 °C for 2 hours. Calcination temperature and time were carefully programmed in a mufla oven. After the thermal treatment, the nanometric powders were obtained.

Phase formation and crystallographic structure were characterized by X-ray diffraction (XRD) on a Rigaku Dmax/2500PC diffractometer using Cu Kα radiation ($\lambda = 1.5406$ Å). The cubic cell parameter and the crystallite size were determined from the FULLPROF software (Version 0.2 Mar 98, LLB Juan Rodriguez-Carvajal). The peak shape was described by a Thompson-Cox-Hastings pseudo-Voigt function. The refinable parameters are the isotropic Lorentzian and Gaussian contribution, respectively, attributed to the size and microstrains. For each diffraction pattern, the Gaussian contribution associated to microstrains was found negative and inferior to 0.4%. Raman spectra were collected (Bruker RFS-100/S Raman spectrometer with Fourier transform). A 1064 nm YAG laser was used as the excitation source, and its power was kept at 150 mW. Fourier transform infrared spectroscopy (FTIR) was recorded using a Bruker Equinox 55 spec-

trometer in diffuse reflection mode. The spectra were measured between 385 and 4000 cm^{-1} region with a resolution of 4 cm^{-1}. Size and morphology of the particles were studied by field emission gun scanning electron microscopy (FEG-SEM). A Zeiss Supra 35-VP microscope was used, operating under a 6 kV incident electron beam. Specimens for transmission electron microscope (TEM) were obtained by drying droplets of as-prepared samples from an ethanol dispersion which had been sonicated for 5 min onto 300 mesh Cu grids. High-resolution transmission electron microscope (HRTEM) images and selected area diffraction (SAD) patterns were then taken to an accelerating voltage of 200 kV on a Philips model CM 200 instrument.

To measure the DC magnetic field, a Hall probe was employed. Magnetization measurements were done by using a vibrating-sample magnetometer (VSM) from Quantum Design™. All measurements were taken at room temperature. Dielectric properties were measured using an impedance analyser, model 4192 of HP. From the capacitance dependence temperature curves, the Curie temperature was determined.

III. Results and discussion

In this presented paper, aluminium substituted YIG, with formula $Y_3Fe_{5-x}Al_xO_{12}$ ($1.5 < x < 1.7$), was prepared by polymeric precursor method. The influence of stoichiometry on phase formation was monitored. The diffraction patterns reveals that yttrium aluminium iron garnet appears as a single phased for all stoichiometries at 700 °C. The Bragg peaks are in accordance with the literature [29], proving that the particles are pure and homogenous. X-ray diffraction patterns reveal that the structure of powders is *bcc* and the garnet phase has been obtained after calcining. Small shifts of diffraction lines of Bragg angles with increasing the Al concentration were observed. This is due to the fact that the radius of Al^{3+} is 0.5 Å and that of Fe^{3+} is 0.61 Å [29], and by substitution of Al^{3+} instead of Fe^{3+} slight changes of lattice parameter would be expected. From the Fig. 1 it was clear that the 2θ position of each crystal plane showed almost no differences with respect to the doping concentration of Fe^{3+}, implying that the crystal planes were not damaged by doping. Y, Al and O were still in their own original plane. Doping just replaced a Fe^{3+} ion with an Al^{3+} ion without changing the whole crystal structure. The average crystallite size of different samples was in the range 46–65 nm. Lattice parameters were 1.2280, 1.2265 and 1.2260 nm for x value equal to 1.5, 1.6 and 1.7, respectively.

FT-IR spectrums for the powders are shown in Fig. 2. The presence of multiple bonds in the $Y_3Fe_{5-x}Al_xO_{12}$ powders can be noticed. All powders analysed presented O–H bond stretching from 3200 to 3600 cm^{-1}, probably due to water absorption during test. Wavenumbers ranging from 825 to 930 cm^{-1} represent axial strain of C–O bonds in carbonates and carboxylates, respectively, proving the presence of these compounds in the samples. Wavenumbers ranging from 545 to 680 cm^{-1} are assigned to stretching mode of YIG tetrahedra [15], characteristic of metal-oxygen bonds in ceramics. There was, however, a vibration band noted that is associated to the deformation of O–H bonds near 1680 cm^{-1}. This is attributed to water adsorbed at the powder surface when the sample was in contact with the environment. The spectrum exhibits three bands at 759, 680 and 602 cm^{-1} assigned to the stretching mode of YIG tetrahedral [30]. In the case of aluminium substituted YIG, these bands are slightly broadened and shifted towards higher wavenumbers. Unlike previous studies [20], IR spectra show very weak bands characteristic of carbonates (1400 and 1520 cm^{-1}). The band at 2339 cm^{-1} was previously assigned by Vaqueiro *et al.* to atmospheric CO_2 [20]. Nevertheless, this band did not disappear after long degassing time and could be assigned to another absorber which nature remains unknown.

Figure 3 shows the Raman spectra of YIG polycrystalline powders with different aluminium doping concentrations. It is already known from X-ray diffraction analyses that there is no crystal structural change

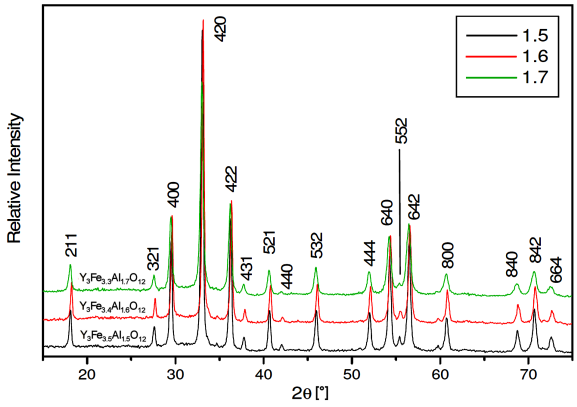

Figure 1. X-ray diffraction pattern of $Y_3Fe_{5-x}Al_xO_{12}$ powders synthesized at 700 °C for 2 h by the polymeric precursor method

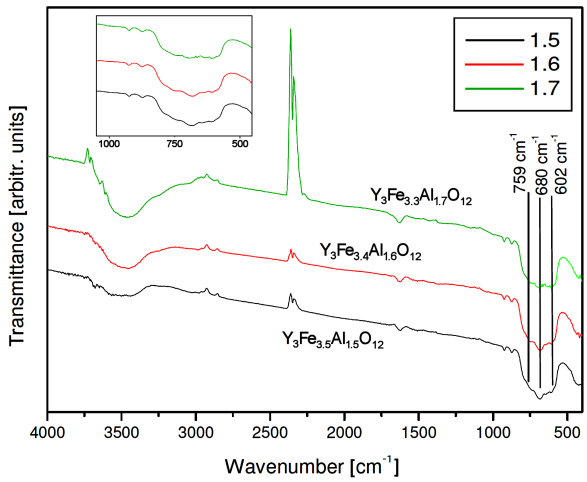

Figure 2. Infrared spectroscopy of $Y_3Fe_{5-x}Al_xO_{12}$ powders synthesized at 700 °C for 2 h by the polymeric precursor method (inset is FT-IR in the range from 500 to 1000 cm^{-1})

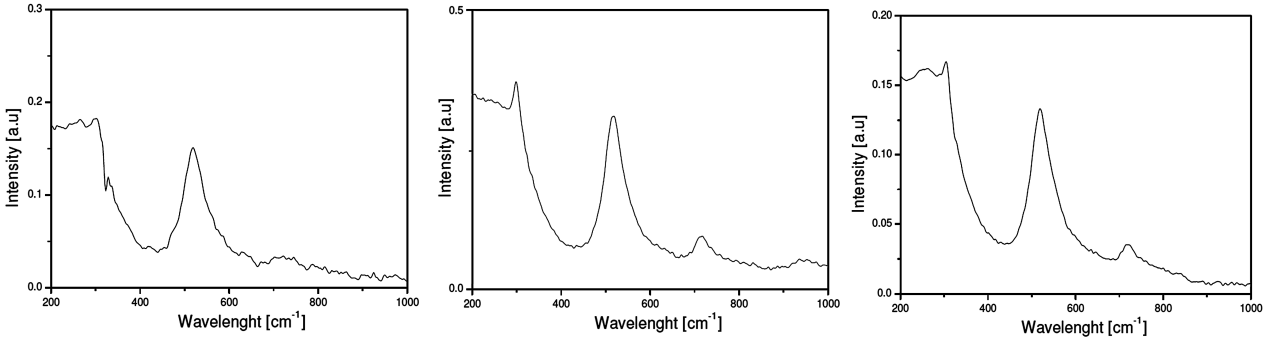

Figure 3. Raman spectra of $Y_3Fe_{5-x}Al_xO_{12}$ powders synthesized at 700 °C for 2 h by the polymeric precursor method with: a) x = 1.5, b) x = 1.6 and c) x = 1.7

in theses powders. However, Raman spectra do show some quite obvious variations in the molecular vibrational modes as the doping concentration is changed. This clearly indicates that Al-doping does replace ions in the crystal, thus changing the original YIG vibrational modes toward the YAG Raman spectrum. We believe that the replaced ions are the central aluminium ions in the tetrahedrons and octahedrons. First, let us examine the peak at 720 cm^{-1}. As the doping concentration is increased, the relative intensities of these peaks are gradually decreased and eventually disappear from the spectrum as aluminium doping is 1.6. This may be explained as follows. As Al^{3+} ions are doped into the YIG crystals, they gradually fill into the tetrahedrons and octahedrons and replace Fe^{3+} as their central ion. The greater mass of Fe^{3+} ion makes the tetrahedrons and octahedrons heavier than before, thus, weakens these vibrations and causes the decrease in their relative intensities. We speculate that there might be a phase change point somewhere in between 1.5 and 1.6 which causes the complete disappearance of these vibrational modes of the aluminium-centred tetrahedrons and octahedrons. As pointed out in the reference [7], these peaks are the internal stretching or external vibrations between aluminium ion and oxygen, or between aluminium-centred tetrahedrons or octahedrons and oxygen. These peaks disappear at high doping concentrations. This may be attributed to the various displacement situations of aluminium by iron. In an YAG crystal, there are 16 octahedral a lattices, each with six coordinating oxygen ions and 24 tetrahedral d lattices, each with four coordinating oxygen ions. Fe^{3+} ion displacement may take place in either one of these lattices. It may be reasonably assumed that ion displacement in these lattices may be sequential. That is, one group may start after the other finishes. Since the Al^{3+} induced vibrational modes give rise to higher peak intensities in this region than those in the previous region, the remaining spectral signals may, therefore, be attributed to those lattices in which their Al^{3+} ions are not yet displaced. The peaks at 300, and 520 cm^{-1} are from vibrations of Y^{3+} ions. No frequency shift is observed as indicated in Fig. 3.

The determination of hydrodynamic particle size was made by mercury porosimetry and is important because most biotechnological processes use liquid media. The observed hydrodynamic particle size (Fig. 4) is larger than the crystallite size and confirms the aggregation phenomenon. The theoretical number of crystallites per particle is determined as the ratio of the hydrodynamic particle size to the crystallite size and it is nearly a constant function of x. The average values are 2.5, 1.8 and 2.0 for x values equal to 1.5, 1.6 and 1.7, respectively. This may be explained by the fact that the samples were calcined at the same temperature and during the same

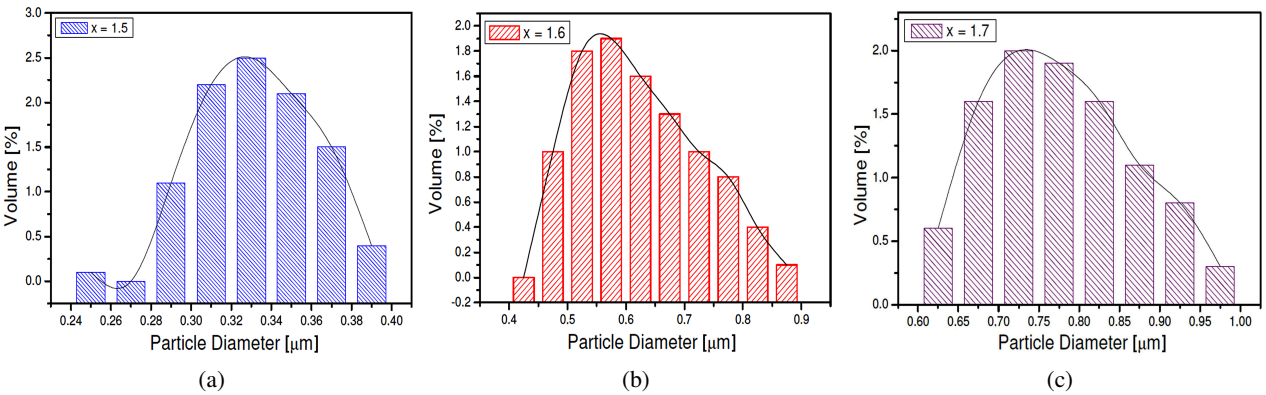

Figure 4. Hydrodynamic particle size distribution of $Y_3Fe_{5-x}Al_xO_{12}$ with: a) x = 1.5, b) x = 1.6 and c) x = 1.7

time and may indicate a constant sintering process. The aluminium substituted YIG powder is composed of particles with a hydrodynamic average diameter particle size of approximately 0.3, 0.6 and 0.8 μm for x value equal to 1.5, 1.6 and 1.7, respectively.

Field emission gun scanning electron microscope (FEG-SEM) was used for better evaluation of the $Y_3Fe_{5-x}Al_xO_{12}$ nanoparticles prepared by polymeric precursor method (Fig. 5). The particles are present in agglomerates, independently of the stoichiometry. Obviously, the obtained solids are composed of grains with no regular shape. For example, the volumetric plate-like grains coexist with spherically shaped particles, and they are partially fused to form hard agglomerates. Particles' morphology is similar for all compositions, but the agglomerates seem to enlarge as the Fe/Al ratio decreases. Afterwards, it is possible to separate the particles by ball milling in order to reduce the size of the agglomerates and increase the specific area. It is interesting to note that almost identical microstructure was observed for all samples. As the Fe/Al ratio decreases individual particles seem to be plate-like crystals with an average particle size of around 0.3 μm.

Figure 6 shows a bright field image of the sample (on the left), and corresponding selected area electron diffraction pattern (on the right). In the electron micrograph, grain-like particles with dimensions ranging from several nanometers to several tens of nanometers are observed. Compared to hydrodynamic average diameter, particles with lower size were observed specially due to the agglomerates. It should be noted that it was possible to separate particle with size between 10 and 100 nm after 30 min of centrifugation at a constant rotation speed.

As the specimen was tilted with respect to the incident electron beam, image contrast for several particles changed significantly, suggesting that these particles were crystalline in nature. SAD shows predominantly a halo pattern in a small diffraction angle region. There are diffraction rings together with several weak spots present. This indicates that the majority of the particles were still in the crystalline form, but the symmetry of unit cells slightly changed. Although the exact mechanism of the phase formation of $Y_3Fe_{5-x}Al_xO_{12}$ with $1.5 < x < 1.7$ garnets has not yet been identified, the common feature of both their synthesis and magnetic properties of the crystalline YIG has play special importance. In almost all regions of the specimen, agglomerates were observed, whereas the small particles were dispersed on exceptionally small fraction of the total area. It is therefore concluded that the particles are crystalline and consistent with the results from X-ray diffraction, leading to the conclusion that no intermediate state exists between the amorphous and the crystalline YIG. Otherwise, the diffraction pattern of YIG structure becomes disordered as Fe/Al ratio decreases. It should, however, be noted that the diffraction spots do not exactly fall on the circumference of the diffraction rings but fluctuate with respect to the radial direction. This fluctuation was not observed in the X-ray diffraction patterns.

In order to understand the role of aluminium in the substituted garnet a study of magnetic properties was undertaken. Figure 7 shows hysteresis loops of $Y_3Fe_{5-x}Al_xO_{12}$ samples thermal treated at 700 °C for 2 h at room temperature. In the YIG, the A = Y^{3+} site is eightfold dodecahedrally coordinated (c site), the B = Fe^{3+} site six-fold octahedral (a site) and the B_0 = Fe^{3+} site four-fold tetrahedral (d site). Y^{3+} is diamagnetic and the magnetic moment results from negative superexchange (antiferromagnetic) interaction between Fe^{3+} ions in these two different a and d sites. In this case, the a–d interactions are dominant compared to a–a and d–d interactions [23]. As it can be seen, the particles are superparamagnetic. Fe^{3+} ions occupy tetrahedral (d) and octahedral (a) sites antiferromagnetically, therefore, the magnetic moment is a response to the negative superexchange interaction between Fe^{3+} in a and d sites [15]. At first, Al^{3+} ions preferably substitutes Fe^{3+} ions in d sites for small quantities, and tend to octahedral substitution as Al^{3+} concentration is increased [6]. As Fe^{3+} ions are substituted by the non-magnetic Al^{3+} ions in d and a sites the superexchange interactions of iron ions in the lattice is reduced [6], consequently reducing the magnetization, as it can be seen for lower Fe/Al ratios. As it is well known, tetrahedral site is smaller than octahedral site. In substituted YIG a non-magnetic substituent M^{3+} ion occupies predominantly an octahedral or tetrahedral site for small x as it is larger than Fe^{3+}. In other words, the smaller ion persistently seeks a smaller site [31]. Reduction of magnetization for higher Al^{3+} concentration is due to the substitution of Fe^{3+} for Al^{3+} in octahedral and tetrahedral sites in substituted YIG and the reduction of super exchange interactions in the lattice. The percentage efficiency calculated from hysteresis loops are 91.4%, 93.7% and 95.9% for x equal to 1.5, 1.6 and 1.7, respectively. Therefore, the efficiency seems to increase as Fe/Al ratio decreases. However, less energy is converted to heat as Fe/Al ratio decreases, once the magnetization saturation is proportional to the presence of Fe^{3+} ions in the compound.

The temperature dependence of dielectric permittivity is shown in Fig. 8. The dielectric permittivity measured at 10 kHz are 14300, 11600 and 4660 for x equal to 1.5, 1.6 and 1.7, respectively, and the phase transitions are around 53, 47 and 37 °C. A structural phase transition corresponds to the transition of a non polar state to a polar state at T_c. The dielectric permittivity increases gradually with an increase in temperature up to the transition temperature (T_c) or Curie point and then decreases. Also, the maximum dielectric permittivity (ε_m) and the corresponding maximum temperature (T_m), depend on the composition. The magnitude of the dielectric permittivity decreases for $Y_3Fe_{3.5}Al_{1.5}O_{12}$ to $Y_3Fe_{3.4}Al_{1.6}O_{12}$ and $Y_3Fe_{3.3}Al_{1.7}O_{12}$, respectively, and the Curie temperature shifts toward a lower temperature

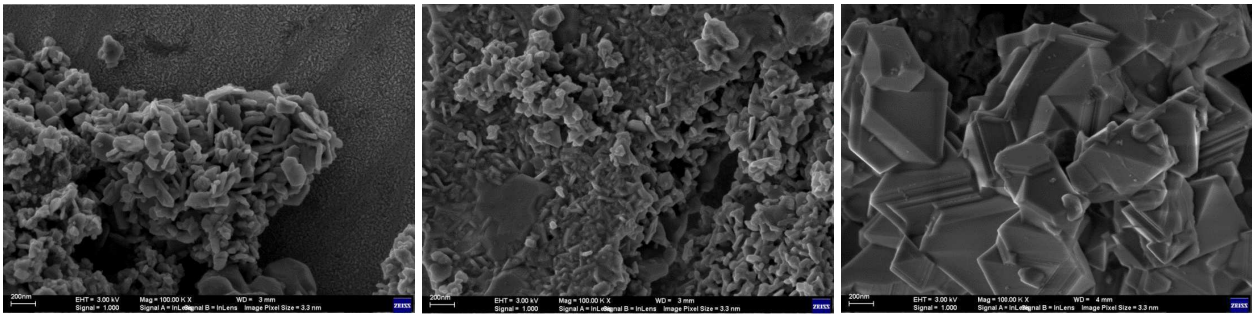

(a) (b) (c)

Figure 5. FEG-SEM of $Y_3Fe_{5-x}Al_xO_{12}$ powders synthesized at 700 °C for 2 h by the polymeric precursor method with: a) x = 1.5, b) x = 1.6 and c) x = 1.7

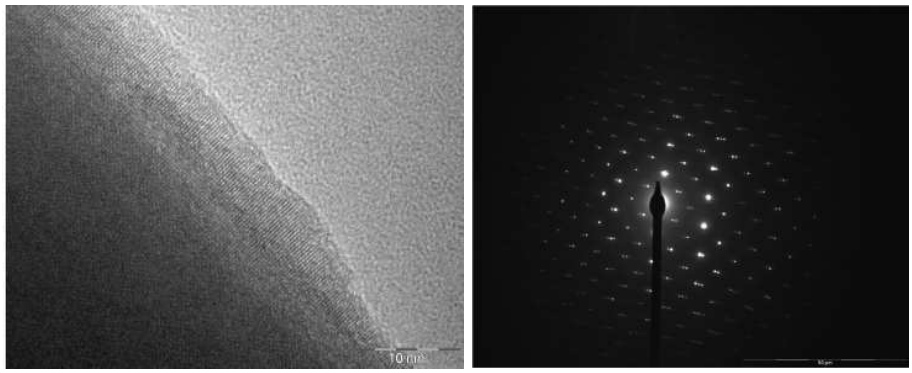

(a)

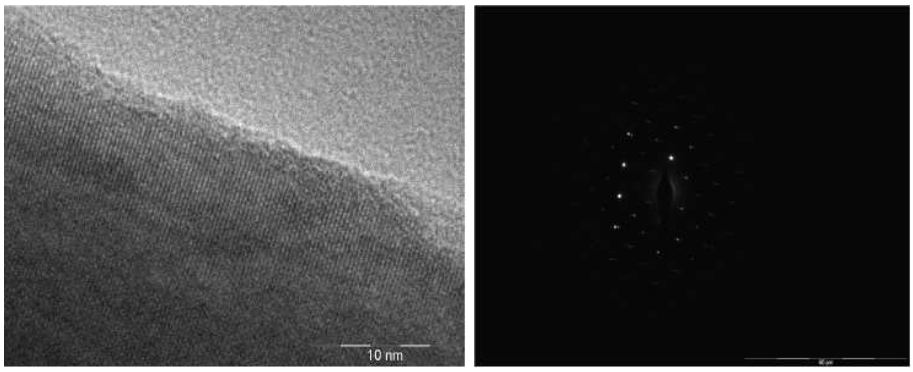

(b)

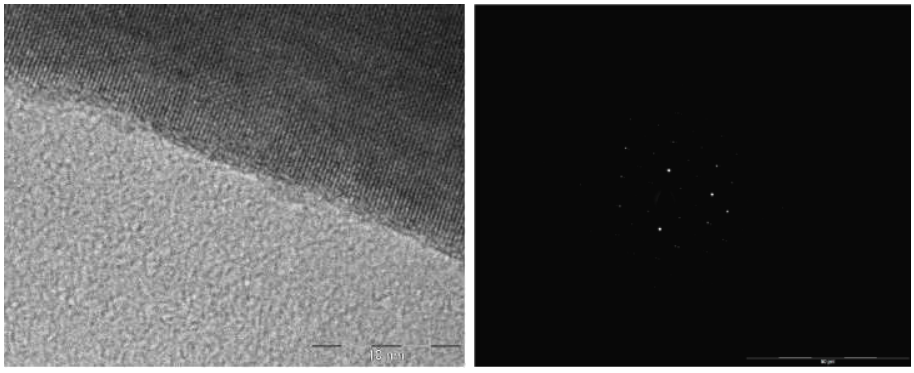

(c)

Figure 6. TEM and SAD images of $Y_3Fe_{5-x}Al_xO_{12}$ powders synthesized at 700 °C for 2 h by the polymeric precursor method with: a) x = 1.5, b) x = 1.6 and c) x = 1.7

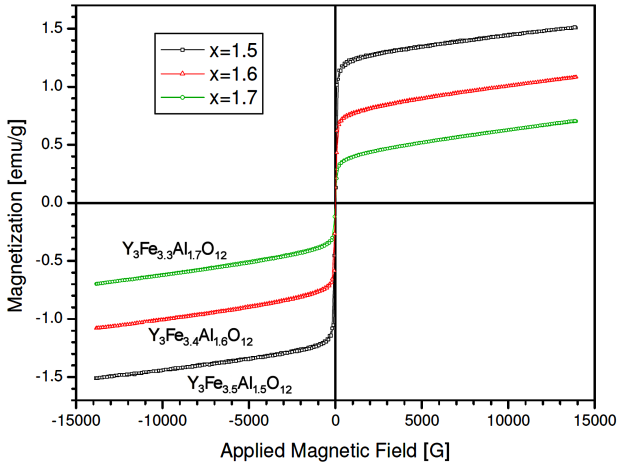

Figure 7. M-H loops of $Y_3Fe_{5-x}Al_xO_{12}$ powders synthesized at 700 °C for 2 h by the polymeric precursor method

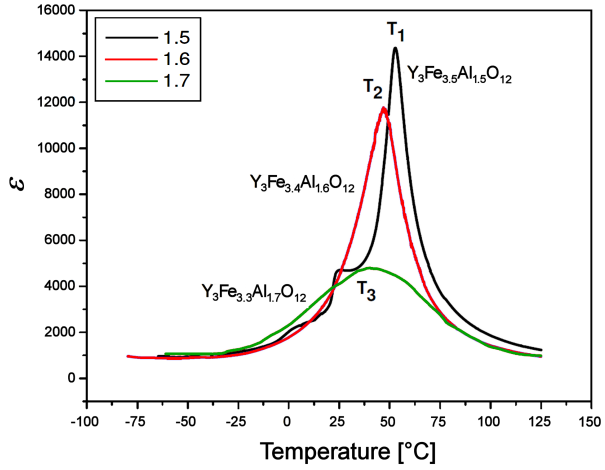

Figure 8. Temperature dependence of dielectric permittivity at 10 KHz of $Y_3Fe_{5-x}Al_xO_{12}$ ($1.5 < x < 1.7$) powders synthesized at 700 °C for 2 h by the polymeric precursor method

which indicates that dielectric polarization is a relaxation type in nature. The region around the dielectric peak is broadened due to a disorder in the cations arrangement in one or more crystallographic sites of the structure. The reduction of dielectric permittivity indicates that Al^{3+} ions are doped into the YIG crystals, they gradually fill into the tetrahedrons and octahedrons and replace Fe^{3+} as their central ion. The higher the aluminium content is, the lower the Curie temperature is because the number of the main magnetic interaction J_{ad} (where J_{ad} is the constant exchange between cations in *a* and *d* sites) per magnetic ion per formula was reduced. So in the composition range investigated, T_c values are near room temperature. To improve confiability, temperature-dependent magnetization curves and differential scanning calorimetry (DSC) should be performed.

IV. Conclusions

$Y_3Fe_{5-x}Al_xO_{12}$ (YIG, with $1.5 < x < 1.7$) nanoparticles with no impurities were synthesized by the polymeric precursor method at 700 °C for 2 h. XRD patterns suggest that the powder crystallizes in *bcc* garnet structure and doping just replaced a Fe^{3+} ion with an Al^{3+} ion. Raman analysis revealed that as Al^{3+} ions are doped into the YIG crystals, they gradually fill into the tetrahedrons and octahedrons and replace Fe^{3+} as their central ion. Field emission electron scanning microscopy shows particles' morphology similar for all compositions, but the agglomerates seem to enlarge as the Fe/Al ratio decreases. Transmission electron microscopy and selection area diffraction evidenced disordered structure as Fe/Al ratio decreases and that almost all YIG particles are crystalline. Particles' efficiency increases as Fe/Al ratio decreases, ranging from 91.4% to 95.9%. The reduction of magnetization for higher Al^{3+} concentration is due to the substitution of Fe^{3+} for Al^{3+} in octahedral and tetrahedral sites in substituted YIG and the reduction of super exchange interactions in the lattice. Variation of T_c showed that Al substitution leads to the reduction of the Curie temperature.

Acknowledgments: The financial support of this research project by the Brazilian research funding agencies CNPq 573636/2008-7, INCTMN 2008/57872-1 and FAPESP 2013/07296-2. We would like to thank Professor Elson Longo for facilities.

References

1. V.F. Castro, J. Celestino, A.A.A. Queiroz, F.G. Garcia, "Propriedades magnéticas e biocompatíveis de nanocompósitos para utilização em magneto-hipertermia", *Revista Brasileira de Física Médica*, **4** [1] (2010) 79–82.
2. A.E. Deatsch, B.A. Evans, "Heating efficiency in magnetic nanoparticle hyperthermia", *J. Magn. Magn. Mater.*, **354** (2104) 163–172.
3. E.D. Passos, "Síntese e Caracterização de Microesferas Magnéticas para Utilização em Hipertermia", Dissertação (Mestrado em Materiais) - Universidade Federal de Itajubá, Itajubá, 2006.
4. R.K. Gilchrist, R. Medal, W.D. Shorey, R.C. Hanselman, J.C. Parrot, C.B. Taylor, "Selective inductive heating of lymph nodes", *Ann. Surg. Oncol.*, **146** [4] (1957) 596–606.
5. C.S.S.R. Kumar, F. Mohammad, "Magnetic nanomaterials for hyperthermiabased therapy and controlled drug delivery", *Adv. Drug Delivery Rev.*, **63** (2011) 789–808.
6. Z.A. Motlagh, M. Mozaffari, J. Amighian, "Preparation of nano-sized Al-substituted yttrium iron garnets by the mechanochemical method and investigation of their magnetic properties", *J. Magn. Magn. Mater.*, **321** (2009) 1980–1984.
7. F. Bertaut, F. Forrat, "Structure des ferrites ferrimagnetiques des terres rares", *Compt. Rend.*, **242** (1956) 382.
8. Y.F. Chem, K.T. Wu, Y.D. Yao, C.H. Peng, K.L. You, W.S. Tse, "The influence of Fe concentration

on $Y_3Fe_{5-x}Al_xO_{12}$ garnets", *Microelectron. Eng.*, **81** (2005) 329–335.
9. W.F.F.W. Ali, M. Othman, M.F. Ain, N.S. Abdullah, Z.A. Ahmad, "Studies on the formation of yttrium iron garnet (YIG) through stoichiometry modification prepared by conventional solid-state method", *J. Eur. Ceram. Soc.*, **33** (2013) 1317–1324.
10. Z. Cheng, H. Yang, "Synthesis and magnetic properties of Sm-$Y_3Fe_5O_{12}$ nanoparticles", *Physica E*, **39** (2007) 198–202.
11. Z.A. Motlagh, M. Mozaffari, J. Amighian, A.F. Lehlooh, M. Awawdeh, S. Mahmood, "Mössbauer studies of $Y_3Fe_{5-x}Al_xO_{12}$ nanopowders prepared by mechanochemical method", *Hyperfine Interact*, **198** (2010) 295–302.
12. M.N. Akhtar, M.A. Khan, M. Ahmad, G. Murtaza, R. Raza, S.F. Shaukat, M.H. Asif, N. Nasir, G. Abbas, M.S. Nazir, M.R. Raza, "$Y_3Fe_5O_{12}$ nanoparticulate garnet ferrites: Comprehensive study on the synthesis and characterization fabricated by various routes", *J. Magn. Magn. Mater.*, **368** (2014) 393–400.
13. R. Hergt, S. Dutz, R. Muller, M. Zeisberger, "Magnetic particle hyperthermia: Nanoparticle magnetism and materials development for cancer therapy", *J. Phys.: Condens. Matter*, **18** (2006) S2919–S2934.
14. M.N. Akhtar, M.A. Khan, M.R. Raza, M. Ahmad, G. Murtaza, R. Raza, S.F. Shaukat, M.H. Asif, M. Saleem, M.S. Nazir, "Structural, morphological, dielectric and magnetic characterizations of $Ni_{0.6}Cu_{0.2}Zn_{0.2}Fe_2O_4$ (NCZF/MWCNTs/PVDF) nanocomposites for multilayer chip inductor (MLCI) applications", *Ceram. Int.*, **40** (2014) 15821–15829.
15. F. Grasset, S. Mornet, A. Demourgues, J. Portier, J. Bonnet, A. Vekris, E. Duguet, "Synthesis, magnetic properties, surface modification and cytotoxicity evaluation of $Y_3Fe_{5-x}Al_xO_{12}$ ($0 \leq x \leq 2$) garnet submicron particles for biomedical applications", *J. Magn. Magn. Mater.*, **234** (2001) 409–418,.
16. H. Yu, L. Zeng, C. Lu, W. Zhang, G. Xu, "Synthesis of nanocrystalline yttrium iron garnet by low temperature solid state reaction", *Mater. Charact.*, **62** (2011) 378–381.
17. D.T.T. Nguyet, N.P. Duong, T. Satoh, L.N. Anh, T.D. Hien, "Temperature-dependent magnetic properties of yttrium iron garnet nanoparticles prepared by citrate sol-gel", *J. Alloys Compd.*, **541** (2012) 18–22.
18. Y-P. Fu, C-H. Lin, K-Y. Pan, "Microwave-induced combustion synthesis of yttrium iron garnet nanopowders and their characterizations", *J. Magn. Magn. Mater.*, **272-276** (2004) 2202–2204.
19. P. Grosseau, A. Bachiorrini, B. Guilhot, "Preparation of polycrystalline yttrium iron garnet ceramics", *J. Therm. Anal.*, **46** (1996) 1633–1644.
20. P. Vaqueiro, M.A. Lopez-Quintela, J. Rivas, "Synthesis of yttrium iron garnet nanoparticles via coprecipitation in microemulsion", *J. Mater. Chem.*, **7** (1997) 501–504.
21. S. Taketomi, Y. Ozaki, K. Kawasaki, S. Yuasa, H. Miyajima, "Transparent magnetic fluid: preparation of YIG ultrafine particles", *J. Magn. Magn. Mater.*, **122** (1993) 6–9.
22. M. Inoue, T. Nishikawa, T. Inui, "Glycothermal synthesis of rare earth iron garnets", *J. Mater. Res.*, **13** (1998) 856–860.
23. D. Bahadur, B. Sharma, D. Chakravorty, "Preparation of glass-ceramics containing YIG", *J. Mater. Sci. Lett.*, **1** (1982) 106–108.
24. M.P. Pechini, "Method of preparing lead and alkaline earth titanates and niobates and coating method using the same to form a capacitor", US Pattent. No 3 330 697, July 11, 1967.
25. A.Z. Simões, A.H.M. Gonzalez, M.A. Zaghete, J.A. Varela, B.D. Stojanovic, "Preparation of 9/65/35 PLZT thin films deposited by a dip-coating process", *J. Eur. Ceram. Soc.*, **31** (2001) 168–174.
26. M.H. Farou, "Método Pechini para Preparação de Nanopartículas", IX Semana de Estudos de Física da Unicentro, Guarapuava, Paraná, 2011.
27. A.A. Cavalheiro, M.A. Zaghete, J.A. Varela, "Influência do oxalate de amônio na formação do precursor columbita obtido pelo método Pechini", *Cerâmica*, **45** [292-293] (1999) 56–60.
28. A.Z. Simões, M.A. Ramirez, N.A. Perucci, C.S. Riccardi, E. Longo, J.A. Varela, "Retention characteristics in $Bi_{3.25}La_{0.75}Ti_3O_{12}$ thin films prepared by the polymeric precursor method", *Appl. Phys. Lett.*, **86** (2005) 112909.
29. C.S. Kim, B.K. Min, S.J. Kim, S.R. Yoon, Y.R. Uhm, "Crystallographic and magnetic properties of $Y_3Fe_{5-x}Al_xO_{12}$", *J. Magn. Magn. Mater.*, **254-255** (2003) 553–555.
30. A.M. Hofmeister, K.R. Campbell, "Infrared spectroscopy of yttrium aluminum, yttrium gallium and yttrium iron garnets", *J. Appl. Phys.*, **72** (1992) 638–646.
31. M.A. Gilleo, S. Geller, "Magnetic and crystallographic properties of substituted yttrium-iron garnet, $3\,Y_2O_3{\cdot}xM_2O_3{\cdot}(5\text{-}x)Fe_2O_3$", *Phys. Rev.*, **110** (1958) 73–77.